Secrecy Performance of Multi-Antenna Satellite-Terrestrial Relay Networks with Jamming in the Presence of Spatial Eavesdroppers

Xiaoqi Wang[1], Zheng Hou[1], and Hanwei Zhang[2*]
[1] School of Surveying and Land Information Engineering, Henan Polytechnic University
Jiaozuo 454003, China
[e-mail: wangxiaoqi@hpu.edu.cn]
[2] Institute of Resources & Environment, Henan Polytechnic University
Jiaozuo 454003, China
[e-mail: zh_hpu@163.com]
*Corresponding author: Hanwei Zhang

Abstract

This work investigates the physical layer secrecy of a multi-antenna hybrid satellite-terrestrial relay networks (HSTRN) with jamming, in which a satellite aims to make communication with a destination user by means of a relay, along with spatially random eavesdroppers. In order to weaken the signals of eavesdroppers, the conventional relay can also generate intentional interference, besides forwarding the received signal. Shadowed-Rician fading is adopted in satellite link, while Rayleigh fading is adopted in terrestrial link, eavesdropper link and jamming link. The analytical and asymptotic formulas for the system secrecy outage probability (SOP) are characterized. Practical insights on the diversity order of the network are revealed according to the asymptotic behavior of SOP at high signal-to-noise ratio (SNR) regime. Then, analysis of the system throughput is examined to assess the secrecy performance. In the end, numerical simulation results are presented to validate the theoretical analysis and point out: (1) The secrecy performance of the considered network is affected by the channel fading scenario, the system configuration; (2) Decrease of the relay coverage airspace can provide better SOP performance; (3) Jamming from the relay can improve secrecy performance without additional network resources.

1. Introduction

The ever-increasing demand for high-speed and broadband have stimulated the development of wireless communication. Meanwhile, satellite communication is gaining more attention for its advantage of long distance, large capacity, wide coverage, high quality and low cost [1,2], and it has been applied widely in navigation, location, disaster response, military, resource exploration, topographic mapping and so on [1,3].

Unfortunately, obstacles or shadowing in the satellite-terrestrial communication may cause the inaccessibility of the line-of-sight (LOS) [4], and this will seriously reduce the communication quality of the satellite network. Thus, hybrid satellite-terrestrial relay networks (HSTRN) integrated with satellite-terrestrial communication and relay is proposed [5-8], and it has a bright application prospect because of more diversity gain, wider coverage, better reliability, less power consumption and other advantages [9-11]. This framework has been already included in the standard of DVB-SH [12]. Hence, most research works have focused on different methods to improve the performance of HSTRN [2,13,14]. [2] and [13] investigated the outage performance of their proposed frameworks applying amplify-and-forward (AF) and decode-and-forward (DF) protocol respectively. [14] derived the average symbol error rate (ASER) and the diversity order of the HSTRN with co-channel interferes (CCI) using moment generating function (MGF), and demonstrated the impact of CCI on the system performance.

On the other hand, given that multiple-input-multiple-output (MIMO) technology in terrestrial networks can obtain more diversity gain, further interest has risen in the possibility of applying the same principle to satellite networks. Therefore, more and more research efforts have been performed on incorporating MIMO technology into satellite networks with multiple antennas in [15,16]. [15] investigated a multi-antenna AF relaying scheme, and revealed that the number of transmit and receive antennas has impacts on the outage performance and ergodic capacity of the system. Researchers of [16] assumed a multi-antenna HSTRN corrupted by multiple CCI at relay and destination, indicating that the performance degradation of the HSTRN was resulted from CCI through reducing the array gain.

As is known to all, the security performance is a very important problem in the development of wireless communication. Comparing to traditional encryption method at upper layers, physical layer secrecy has become a popular approach for its advantage of preventing information delivery from eavesdropping [17]. And research on physical layer secrecy in HSTRN has become an attractive concern [18-20]. [18] gave a performance comparison of AF and DF HSTRN based on multi-antenna relay, and indicated that the proposed DF HSTRN always had a better secrecy performance than AF HSTRN. [19] considered a HSTRN composed of a multi-antenna satellite, multiple relays and users with multiple eavesdroppers, and presented a selection rule of best user-relay pair aiming at minimizing secrecy outage probability(SOP). In [20], authors investigated a multi-hop HSTRN, and characterized accurate and asymptotic expressions for SOP to explore the physical layer secrecy performance. And on this basis, relays or even the destinations themselves can be used to help provide additional jamming to confuse the eavesdropper. This approach termed as cooperative jamming has been explored in lots of works. In order to protect the message from wiretapping in a HSTRN, [21] investigated power allocation schemes to optimize the secrecy rate with constraint of entire relay power by means of jamming. The same to optimize the secrecy rate, [22] jointly optimized the beamforming vector of relay as well as the covariance matrix of artificial noise. [23] explored a selection of joint relay and a scheme of user scheduling with jamming so as to obtain the balance of the performance and implementation. Considering of

eavesdroppers in the airspace, [24] presented a communication network with unmanned aerial vehicle (UAV) in existence of spatial eavesdroppers, and gave an investigation of physical layer secrecy.

In general, most researches have focused on physical layer secrecy of HSTRN ignoring the spatial distribution of eavesdroppers. While in practical scenarios, the positions of eavesdroppers may vary in different conditions. That will affect the eavesdropper link quality, and then affect the security performance of the entire network. In addition, multi-antenna technology is favored as a MIMO technology with satellite communication, and jamming signal can be used to degrade the eavesdropper link. In light of the above discussion, the secrecy performance analysis of a multi-antenna HSTRN with jamming is investigated in this work, in which a multi-antenna satellite aims to make a communication with a multi-antenna ground user via a relay in exist of spatially random eavesdroppers. The relay here can not only forward the signal using DF protocol, but also generate intentional jamming to eavesdroppers simultaneously. Shadowed-Rician fading is considered for satellite link [25] while Rayleigh fading for terrestrial link, eavesdropper link and jamming link [14]. The main works can be summarized as:

 (1) A multi-antenna HSTRN with jamming was proposed. Considering the spatial random distribution of eavesdroppers, the probability density function (PDF) and the cumulative distribution function (CDF) of eavesdropper link SNR are derived;

(2) In the basis of the proposed network, the analytical and asymptotic formulas for the SOP are deduced;

(3) The diversity order of the network is obtained according to the asymptotic behavior of SOP and the system throughput is explored;

(4) Numerical simulations are operated to validate the correctness of the theoretical analysis, revealing that the secrecy performance of the considered HSTRN relies on its some key parameters.

The contents of this work are organized as the following layouts. Section 2 describes the models of the system and channel. Section 3 investigates the secrecy performance of the network, deriving formulas of the theoretical, asymptotic SOP, and exploring the system throughput. Computer simulation and numerical results are included in Section 4. Conclusion is given in Section 5.

Notations: Vectors are characterized by lowercase bold letters. $(\bullet)^{\dagger}$ means conjugate transpose; $\|\bullet\|$ means Frobenius norm; $|\bullet|$ delegates absolute value; $E[\bullet]$ represents expectation operator; $n!$ denotes factorial; $(\bullet)_n$ symbolizes the Pochhammer symbol; $f_X(\bullet)$ and $F_X(\bullet)$ represent PDF and CDF; $\Pr(\bullet)$ symbolizes the probability of a variable.

2. HSTRN Description
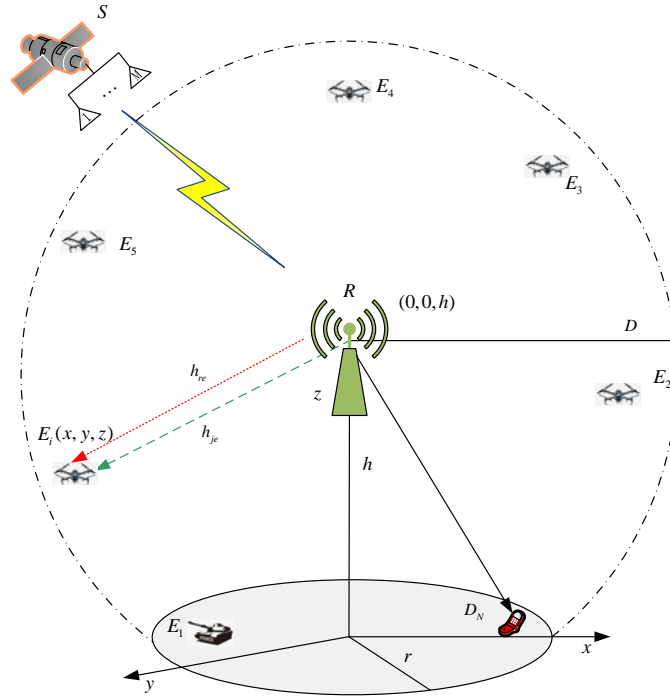
2.1 System Model

Fig. 1. Model of the multi-antenna HSTRN with Spatial Eavesdroppers.

Considering the configuration of a multi-antenna HSTRN is presented in **Fig. 1**, where one geostationary (GEO) satellite source (S) aims to make communication with a terrestrial destination user (D_N) through a DF relay (R), along with a group of eavesdroppers (E). The eavesdroppers distributed randomly in the space or on the ground try to eavesdrop the information from satellite S to the terrestrial user over an eavesdropper channel. Here we assume that each node operates in half-duplex mode. The satellite S and the terrestrial user (D_N) are installed with M and N antennas, and the relay (R) is deployed at the vertical height h, with a single antenna. Here assuming that D_N is located in a circle with a radius of r . During the long satellite-terrestrial communication, clouds, hills, mountains and other obstacles or shadowing cause masking effect, which will lead to the unavailability of LOS communication, and then seriously degrade the performance of the satellite communication. Based on this, assuming that there is no direct link in $S-D_N$ and $S-E$ [2,26,27]. All the nodes in this network are affected by the additive white Gaussian noise (AWGN) (variance denoted with σ^2).

In view of one relay, the communication process can be separated into two transmission phases.

In the first phase, the satellite source beamforms the signal $x_s(t)$ ($E\left[\left|x_s(t)\right|^2\right]=1$) to the relay applying maximum ratio transmission (MRT) principle, so the received signal of the relay can be shown as

$$y_r = \sqrt{P_s}\mathbf{h}_{sr}^{\dagger}\mathbf{w}_{sr}x_s + n_r, \tag{1}$$

where P_s means the transmit power at S, $\mathbf{h}_{sr} \in \mathbb{C}^{M\times 1}$ represents the channel coefficient vector

of $S - R$, $\mathbf{w}_{sr} \triangleq \dfrac{\mathbf{h}_{sr}}{\|\mathbf{h}_{sr}\|}$ ($\mathbf{w}_{sr} \in \mathbb{C}^{M\times 1}$), is the $M \times 1$ transmit weight vector, and n_0 denotes the

AWGN at R [15].

Thus the received SNR of the signals at R can be obtained as

$$\gamma_{sr} = \eta_s \|\mathbf{h}_{sr}\|^2 \tag{2}$$

where $\eta_s = \dfrac{P_s}{\sigma^2}$.

In the second phase, as a conventional relay, it can forward its signal received to the terrestrial user applying DF protocol. The DF protocol is used here because it can remove the channel effects from the first phase on the received signal in the second phase. Otherwise, as a jammer, the relay performs can not only forward the fully decoded signal to the terrestrial user, but also simultaneously transmit intentional interference using parts of its own power. In the meantime, the eavesdropper also intends to wiretap the signal from the relay. In this work, it is assumed that jamming signal is cognized by the legitimate destination according to the apriori knowledge, and hence the jamming effect can be eliminated when decoding the received signal [28]. Considering the jamming signal as well as the unavailability of $S - D$ and $S - E$, the signal received at the destination based on the principle of maximum ratio combining (MRC) can be formulated as

$$y_d = \sqrt{P_r}\mathbf{w}_{rd}^{\dagger}\mathbf{h}_{rd}x_0 + \mathbf{w}_{rd}^{\dagger}\mathbf{n}_d, \tag{3}$$

and signal received at the eavesdropper is expressed as

$$y_e = \sqrt{P_r}h_{re}x_0 + \sqrt{P_j}h_{je}x_0 + n_e, \tag{4}$$

where P_r represents the transmit power at R, $\mathbf{h}_{rd} \in \mathbb{C}^{N\times 1}$ is the channel coefficient vector of

$R - D_N$, $\mathbf{w}_{rd} \triangleq \dfrac{\mathbf{h}_{rd}}{\|\mathbf{h}_{rd}\|}$ ($\mathbf{w}_{rd} \in \mathbb{C}^{M\times 1}$), is the $N \times 1$ receive weight vector, and $\mathbf{n}_d \in \mathbb{C}^{N\times 1}$ is the

$N \times 1$ AWGN vector at D_N [15].

Thus the instantaneous received SNR of the signals at D_N and E can be obtained as

$$\gamma_{rd} = \eta_r \|\mathbf{h}_{rd}\|^2 \tag{5}$$

and

$$\gamma_e = \frac{P_r|h_{re}|^2}{P_j|h_{je}|^2 + \sigma^2} = \frac{\gamma_{re}}{\gamma_{je} + 1}, \tag{6}$$

where $\gamma_{re} = \eta_r|h_{re}|^2$ and $\gamma_{je} = \eta_j|h_{je}|^2$, with $\eta_r = \dfrac{P_r}{\sigma^2}$ and $\eta_j = \dfrac{P_j}{\sigma^2}$.

2.2 Channel Model

According to most of the previous literatures [15,25], the satellite link undergoes the independent shadowed-Rician distribution. The PDF of $|h_{sr}|^2$ is expressed as

$$f_{|h_{sr}|^2}(x) = \alpha_s \sum_{k=0}^{m_s} \zeta(k)x^k e^{-(\beta_s - \delta_s)x}, \tag{7}$$

where $\alpha_s = (2b_s m_s / (2b_s m_s + \Omega_s))^{m_s} / 2b_s$, $\beta_s = 1/2b_s$, $\delta_s = \Omega_s / 2b_s (2b_s m_s + \Omega_s)$ and $\zeta(k) = (-1)^k (1-m_s)_k \delta_s^k / (k!)^2$, b_s being multipath components, m_s being fading severity parameter and δ_s being LOS average power.

Theorem 1: The PDF and CDF of γ_{sr} following Shadowed-Rician fading are given as

$$f_{\gamma_{sr}}(x) = \sum_{k_1=0}^{m_s-1} \cdots \sum_{k_M=0}^{m_s-1} \frac{\Xi(M)}{\eta_s^{\phi}} x^{\phi-1} e^{-(\frac{\beta_s-\delta_s}{\eta_s})x} \tag{8}$$

and

$$F_{\gamma_{sr}}(x) = 1 - \sum_{k_1=0}^{m_s-1} \cdots \sum_{k_M=0}^{m_s-1} \frac{\Xi(M)}{\eta_s^{\phi}} \sum_{p=0}^{\phi-1} \frac{\Gamma(\phi)}{p!} (\frac{\beta_s-\delta_s}{\eta_s})^{-(\phi-p)} x^p e^{-(\frac{\beta_s-\delta_s}{\eta_s})x} . \tag{9}$$

Proof. Let $z = \left|h_{sr_1}\right|^2 + \left|h_{sr_2}\right|^2 + \cdots + \left|h_{sr_{Ns}}\right|^2$, using convolution and recursion, $f_z(z)$ can be obtained as

$$f_z(z) = \sum_{k_1=0}^{m_s-1} \cdots \sum_{k_M=0}^{m_s-1} \Xi(M) z^{\phi-1} e^{-(\beta_s-\delta_s)z} \tag{10}$$

where $\Xi(M) = \alpha_s^M \prod_{i=1}^{M} \zeta(k_i) \prod_{j=1}^{M-1} B\left(\sum_{l=1}^{j} k_l + j, k_{j+1} + 1\right)$, and $\phi = \sum_{i}^{M} k_i + M$.

Making a variable substitution for (7) and after some algebra processing, the PDF of γ_{sr} is deduced as (8). Then integrating the PDF of γ_{sr} , the CDF of γ_{sr} can be formulated as (9).

Given the advantage of Rayleigh distributions in modeling multipath fading with no LOS, Rayleigh fading is considered for the link between the relay and the ground user as well as the eavesdroppers. Importantly, it is applicable for other fading models as well. For the links of $R-D_N$ and $R-E$, the channel coefficient $\left|h_{ri}^*\right|$ ($i = \{d,e,j\}$) follows Rayleigh fading distribution, and the CDF and PDF are respectively formulated as

$$F_{\left|h_{ri}^*\right|^2}(x) = 1 - e^{-\frac{x}{\Omega_i}} \tag{11}$$

and

$$f_{\left|h_{ri}^*\right|^2}(x) = \frac{1}{\Omega_i} e^{-\frac{x}{\Omega_i}} , \tag{12}$$

where Ω_i means the average power of the corresponding transmission link.

Then, take a similar proof of **Theorem 1**, the PDF and CDF of γ_{rd} are calculated respectively as

$$f_{\gamma_{rd}}(x) = \frac{x^{N-1}}{\Gamma(N)(\eta_r \Omega_d)^N} e^{-\frac{x}{\eta_r \Omega_d}} \tag{13}$$

and

$$F_{\gamma_{rd}}(x) = 1 - \sum_{p=0}^{N-1} \frac{x^p e^{-\frac{x}{\eta_r \Omega_d}}}{p!(\eta_r \Omega_d)^p} . \tag{14}$$

For the jamming link, the PDF and CDF of γ_{je} are described as

$$f_{\gamma_{je}}(x) = \frac{1}{\overline{\gamma}_{je}} e^{-\frac{x}{\overline{\gamma}_{je}}} \qquad (15)$$

and

$$F_{\gamma_{je}}(x) = 1 - e^{-\frac{x}{\overline{\gamma}_{je}}} \qquad (16)$$

where $\overline{\gamma}_{je}$ denotes the average SNR of the jamming link.

3. Secrecy Performance Analysis

Secrecy performance investigation is examined in this section, including the theoretical deduction of the SOP formula, the asymptotic behavior analysis of SOP and the exploration of the system throughput.

3.1 SOP Analysis

The instantaneous channel capacity of $S-R$, $R-D_N$ and $R-E$ links can be defined as (17-19), respectively.

$$C_{sr} = \frac{1}{2}\log_2(1+\gamma_{sr}) \qquad (17)$$

$$C_{rd} = \frac{1}{2}\log_2(1+\gamma_{rd}) \qquad (18)$$

$$C_e = \frac{1}{2}\log_2(1+\gamma_e) \qquad (19)$$

And the definition of secrecy capacity is the capacity difference of the legitimate link and eavesdropper link. Given no direct link of $S-E$, the secrecy capacity of $S-R$ and $R-D_N$ link can be represented as (17) and (20).

$$C_d = \left[C_{rd} - C_e\right]^+ = \left[\frac{1}{2}\log_2\left(\frac{1+\gamma_{rd}}{1+\gamma_e}\right)\right]^+, \qquad (20)$$

where $[\bullet]^+ = \max(\bullet, 0)$.

For convenience of analysing, the secrecy SNR is denoted as $\gamma_d = \frac{1+\gamma_{rd}}{1+\gamma_e}$ and (20) can be expressed as

$$C_d = \left[\frac{1}{2}\log_2\gamma_d\right]^+. \qquad (21)$$

For the DF relaying network, secrecy outage will occur when the transmission process in any phase is incompletely decoded or not totally safe. Considering no direct link of $S-D_N$, the secrecy SNR of the overall network is given as

$$\gamma_{sys} = \min\{\gamma_{sr}, \gamma_d\}. \qquad (22)$$

Therefore, the system secrecy outage depends on the weakest phase. Thus the secrecy capacity can be obtained as

$$C_s = \min\{C_{sr}, C_d\}. \qquad (23)$$

Secrecy outage of the network happens as its secrecy capacity C_s is less than a setting secrecy rate threshold C_{th},

$$P_{sec} = \Pr(C_s < C_{th}) . \tag{24}$$

Assuming that all the links are independent of each other, the SOP of the network can be derived as

$$\begin{aligned}
P_{sec} &= \Pr(C_s < C_{th}) = \Pr(\min\{C_{sr}, C_d\} < C_{th}) \\
&= 1 - \left(1 - \Pr(C_{sr} < C_{th})\right)\left(1 - \Pr(C_d < C_{th})\right) \\
&= 1 - \left(1 - \Pr\left(\frac{1}{2}\log_2(1 + \gamma_{sr}) < C_{th}\right)\right)\left(1 - \Pr\left(\frac{1}{2}\log_2 \gamma_d < C_{th}\right)\right), \\
&= F_{\gamma_{sr}}(\gamma_{th} - 1) + \left(F_{\gamma_{sr}}(\gamma_{th} - 1) + 1\right)F_{\gamma_d}(\gamma_{th})
\end{aligned} \tag{25}$$

where $\gamma_{th} = 2^{2C_{th}}$.

Next, we will require $F_{\gamma_{sr}}$ and F_{γ_d} respectively to obtain the SOP of the entire network.

(1) The first phase

The CDF of secrecy SNR γ_{sr} of $S - R$ link can be obtained as (9).

(2) The second phase

During the second phase, the channel coefficient h_{re} from the relay to the eavesdroppers can be expressed as

$$h_{re} = \frac{h_{re}^*}{\sqrt{1 + d_e^{\,v}}} , \tag{26}$$

where d_e denotes the distance between the relay and the eavesdroppers; v represents the path loss exponent; $(0,0,h)$ and $(x,y,0)$ symbolize the coordinates of relay and the eavesdroppers. Thus, the distance d_e can be formulated as

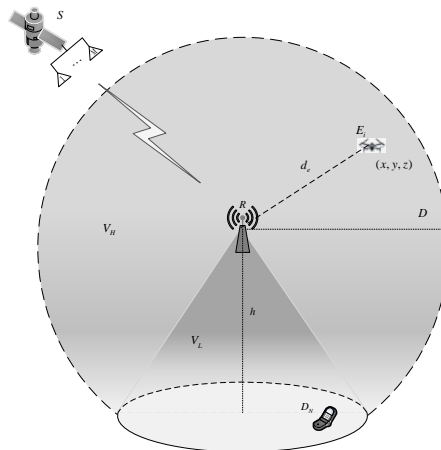$$d_e = \sqrt{x^2 + y^2 + h^2} . \tag{27}$$

Fig. 2. The distribution of d_e.

For briefness, in this work the coverage airspace of the relay is supposed as a sphere with radius D shown in **Fig. 2**. The location of eavesdroppers on the ground or in the air are modeled randomly following an independent homogeneous Poisson point process. To evaluate the performance of eavesdroppers, the distribution of d_e should be obtained first. Therefore, the sphere is divided into two parts V_H and V_L illustrated as **Fig. 2**. The volume proportions of the two parts are respectively formulated as $P_L = \dfrac{(D^2 - h^2)h}{\Xi}$ and $P_H = \dfrac{2D^2(D+h)}{\Xi}$ ($\Xi = 2D^3 + 3D^2h - h^3$).

Theorem 2. *The CDF of d_e is given as below:*

$$F_{d_e}(x) = \begin{cases} 0, & x \le 0 \\ \dfrac{4x^3}{\Xi}, & (0 < x \le h) \\ \dfrac{2x^3 + 3hx^2 - h^3}{\Xi}, & (h < x \le D) \\ 1, & x > D \end{cases}. \tag{28}$$

Proof. In part V_L, when $0 < x \le h$, $F_{d_e}{}^L(x) = \int_0^x \int_{\pi - \arccos\frac{h}{D}}^{\pi} \int_0^{2\pi} \dfrac{3d^2}{\pi\Xi} \sin\phi \, d\theta \, d(d) \, d\phi = \dfrac{(D-h)2x^3}{D\Xi}$,

and when $h < x \le D$,

$F_{d_e}{}^L(x) = \int_{\pi - \arccos\frac{h}{x}}^{\pi} \int_0^{\frac{-h}{\cos\phi}} \int_0^{2\pi} \dfrac{3d^2}{\pi\Xi} \sin\phi \, d\theta \, d(d) \, d\phi + \int_0^x \int_{\pi - \arccos\frac{h}{D}}^{\pi - \arccos\frac{h}{x}} \int_0^{2\pi} \dfrac{3d^2}{\pi\Xi} \sin\phi \, d\theta \, d(d) \, d\phi = \dfrac{3Dhx^2 - 2hx^3 - Dh^3}{D\Xi}$.

Thus, we can obtain (29).

$$F_{d_e}{}^L(x) = \begin{cases} 0, & x \le 0 \\ \dfrac{(D-h)2x^3}{D\Xi}, & (0 < x \le h) \\ \dfrac{3Dhx^2 - 2hx^3 - Dh^3}{D\Xi}, & (h < x \le D) \\ 1, & x > D \end{cases}. \tag{29}$$

In part V_H, $F_{d_e}{}^H(x) = \int_0^x \int_0^{\pi - \arccos\frac{h}{D}} \int_0^{2\pi} \dfrac{3d^2}{\pi\Xi} \sin\phi \, d\theta \, d\phi \, d(d) = \dfrac{2(D+h)x^3}{\Xi D}$. Then, we will obtain (30).

$$F_{d_e}{}^H(x) = \begin{cases} 0, & x \le 0 \\ \dfrac{2(D+h)x^3}{\Xi D}, & 0 < x \le D \\ 1, & x > D \end{cases}. \tag{30}$$

Adding (29) and (30), (28) can be gained.

Then, by derivation of (28), the PDF of d_e is calculated as

$$f_{d_e}(x) = \begin{cases} \dfrac{12x^2}{\Xi}, & (0 < x \le h) \\[2ex] \dfrac{6x^2 + 6hx}{\Xi}, & (h < x \le D). \\[2ex] 1, & else \end{cases} \tag{31}$$

Theorem 3. *The CDF of* γ_{re} *is derived as*

$$F_{\gamma_{re}}(x) = 1 - \frac{6}{\Xi} \sum_{n=0}^{\infty} \frac{(-1)^n}{\left(\overline{\gamma_e}\right)^n n!} \left(\frac{1}{3+vn}\left(h^{3+vn} + D^{3+vn}\right) + \frac{h}{2+vn}\left(D^{2+vn} - h^{2+vn}\right) \right) x^n e^{-\frac{x}{\overline{\gamma_e}}}, \tag{32}$$

where $\overline{\gamma_e} = \eta_r \Omega_e$.

Proof. Based on (12) and (31), using series exploration of $\Upsilon(\cdot,\cdot)$ [29], the CDF of $|h_{re}|^2$ can be deduced as (33).

$$\begin{aligned} F_{|h_{re}|^2}(x) &= \Pr\left(\frac{|h_{re}{}^*|^2}{1+d_e{}^v} \le x \right) = \int_0^D \left(F_{|h_{re}{}^*|^2}\left(x(1+d_e{}^v)\right) \right) f_d(d_e)\, d(d_e) \\[2ex] &= \int_0^h \left(1 - e^{-\frac{x(1+d_e{}^v)}{\Omega_e}} \right) \frac{12d_e{}^2}{\Xi} d(d_e) + \int_h^D \left(1 - e^{-\frac{x(1+d_e{}^v)}{\Omega_e}} \right) \frac{6d_e{}^2 + 6hd_e}{\Xi} d(d_e) \\[2ex] &= 1 - \frac{6e^{-\frac{x}{\Omega_e}}}{\Xi v} \left(\frac{\Upsilon\left(\frac{3}{v}, \frac{x}{\Omega_e}h^v\right)}{\left(\frac{x}{\Omega_e}\right)^{\frac{3}{v}}} + \frac{\Upsilon\left(\frac{3}{v}, \frac{x}{\Omega_e}D^v\right)}{\left(\frac{x}{\Omega_e}\right)^{\frac{3}{v}}} + h\frac{\Upsilon\left(\frac{2}{v}, \frac{x}{\Omega_e}D^v\right)}{\left(\frac{x}{\Omega_e}\right)^{\frac{2}{v}}} - h\frac{\Upsilon\left(\frac{2}{v}, \frac{x}{\Omega_e}h^v\right)}{\left(\frac{x}{\Omega_e}\right)^{\frac{2}{v}}} \right) \end{aligned} \tag{33}$$

Then applying variable substitution and algebra processing, the CDF of γ_{re} is gained as (32).

After derivation of (32), the PDF of γ_{re} is expressed as

$$f_{\gamma_{re}} = \frac{1}{\overline{\gamma_e}} e^{-\frac{x}{\overline{\gamma_e}}} - \sum_{n=1}^{\infty} T\left(nx^{n-1} e^{-\frac{x}{\overline{\gamma_e}}} - \frac{1}{\overline{\gamma_e}} x^n e^{-\frac{x}{\overline{\gamma_e}}} \right), \tag{34}$$

where $T = \frac{6}{\Xi} \frac{(-1)^n}{\left(\overline{\gamma_e}\right)^n n!} \left(\frac{1}{3+vn}\left(h^{3+vn} + D^{3+vn}\right) + \frac{h}{2+vn}\left(D^{2+vn} - h^{2+vn}\right) \right).$

Theorem 4. *The CDF of* γ_d *is formulated as below:*

$$
\begin{aligned}
F_{\gamma_d}\left(\gamma_{th}\right) &= 1 - \sum_{k=0}^{N-1} \frac{\gamma_{th}^k}{k!\left(\eta_r\Omega_r\right)^k} \frac{k!}{\overline{\gamma_e}}\left(\frac{\gamma_{th}}{\eta_r\Omega_r}+\frac{1}{\overline{\gamma_e}}\right)^{-k-1} \\
&\quad - \frac{e^{\frac{1}{\overline{\gamma_{je,l}}}-\frac{2}{\overline{\gamma_{je,l}}(\delta_i+1)}}}{\Gamma(N)\left(\eta_r\Omega_r\right)^N} \frac{\pi\gamma_{th}^N}{2N_0}\sum_{i=0}^{N_0}\left(\frac{(\delta_i+1)}{2}\right)^{N-1}\sqrt{1-\delta_i^2}\frac{N!}{\overline{\gamma_e}}\left(\frac{\gamma_{th}(\delta_i+1)}{2\eta_r\Omega_r}+\frac{1}{\overline{\gamma_e}}\right)^{-N-1} \\
&\quad + \sum_{k=0}^{N-1}\frac{\gamma_{th}^k}{k!\left(\eta_r\Omega_r\right)^k}\sum_{n=1}^{\infty}\mathrm{T}\left(n(k+n-1)!\left(\frac{\gamma_{th}}{\eta_r\Omega_r}+\frac{1}{\overline{\gamma_e}}\right)^{-(k+n)}-\frac{(k+n)!}{\overline{\gamma_e}}\left(\frac{\gamma_{th}}{\eta_r\Omega_r}+\frac{1}{\overline{\gamma_e}}\right)^{-(k+n)-1}\right) \quad (35) \\
&\quad + \frac{e^{\frac{1}{\overline{\gamma_{je,l}}}-\frac{2}{\overline{\gamma_{je,l}}(\delta_i+1)}}}{\Gamma(N)\left(\eta_r\Omega_r\right)^N}\frac{\pi\gamma_{th}^N}{2N_0}\sum_{i=0}^{N_0}\sum_{n=1}^{\infty}\left(\frac{(\delta_i+1)}{2}\right)^{N-1}\sqrt{1-\delta_i^2} \\
&\quad \times \mathrm{T}\left(n(N+n-1)!\left(\frac{\gamma_{th}(\delta_i+1)}{2\eta_r\Omega_r}+\frac{1}{\overline{\gamma_e}}\right)^{-(N+n)}-\frac{(N+n)!}{\overline{\gamma_e}}\left(\frac{\gamma_{th}(\delta_i+1)}{2\eta_r\Omega_r}+\frac{1}{\overline{\gamma_e}}\right)^{-(N+n)-1}\right)
\end{aligned}
$$

Proof. Based on (6), after the approximation $\dfrac{1+x}{1+y}\approx\dfrac{x}{y}$, the PDF of γ_d is derived as

$$
F_{\gamma_d}\left(\gamma_{th}\right)=\Pr\left(\frac{1+\gamma_{rd}}{1+\gamma_e}<\gamma_{th}\right)\approx\Pr\left(\frac{\gamma_{rd}(\gamma_{je}+1)}{\gamma_{re}}<\gamma_{th}\right)=\int_0^{\infty}F_A(\gamma_{th}\gamma_{re})f_{\gamma_{re}}(\gamma_{re})d\gamma_{re}, \quad (36)
$$

where $A=\gamma_{rd}(\gamma_{je}+1)$.

To proceed, $F_A(z)$ is derived as

$$
F_A(z)=\Pr\left(\gamma_{rd}\left(\gamma_{je}+1\right)<z\right)=\int_0^z F_{\gamma_{je}}\left(\frac{z}{\gamma_{rd}}-1\right)f_{\gamma_{rd}}(\gamma_{rd})d\gamma_{rd}=\int_0^z\left(1-e^{-\frac{\frac{z}{x}-1}{\overline{\gamma_{je}}}}\right)\frac{x^{N-1}}{\Gamma(N)\left(\eta_r\Omega_r\right)^N}e^{-\frac{x}{\eta_r\Omega_r}}dx
$$

$$. (37)$$

Invoking (13) and (16) into (37), after algebra processing and approximation based on Gaussian-Chebyshev [30], $F_A(z)$ is derived as (38).

$$
F_A(z)\approx 1-\sum_{k=0}^{N-1}\frac{z^k e^{-\frac{z}{\eta_r\Omega_r}}}{k!\left(\eta_r\Omega_r\right)^k}-\frac{e^{\frac{1}{\overline{\gamma_{je,l}}}}}{\Gamma(N)\left(\eta_r\Omega_r\right)^N}\frac{\pi z^N}{2N_0}\sum_{i=0}^{N_0}\left(\frac{\delta_i+1}{2}\right)^{N-1}e^{-\frac{2}{\overline{\gamma_{je,l}}(\delta_i+1)}-\frac{z(\delta_i+1)}{2\eta_r\Omega_r}}\sqrt{1-\delta_i^2}. \quad (38)
$$

Now, substituting (34) and (38) into (36), and doing some algebra processing, the CDF of γ_d can be obtained as (35).

(3) SOP of the network

Invoking (9) and (35) into (25), the SOP of the entire network is formulated as

$$
P_{\text{sec}} = 1 - \left(\sum_{k_1=0}^{m_s-1} \cdots \sum_{k_M=0}^{m_s-1} \frac{\Xi(M)}{\eta_s^{\phi}} \sum_{p=0}^{\phi-1} \frac{\Gamma(\phi)}{p!} \left(\frac{\beta_s - \delta_s}{\eta_s} \right)^{-(\phi-p)} (\gamma_{th} - 1)^p e^{-\left(\frac{\beta_s - \delta_s}{\eta_s} \right)(\gamma_{th} - 1)} \right)
$$

$$
\times
\begin{pmatrix}
\displaystyle \sum_{k=0}^{N-1} \frac{\gamma_{th}^k}{k!(\eta_r \Omega_r)^k} \frac{k!}{\overline{\gamma_e}} \left(\frac{\gamma_{th}}{\eta_r \Omega_r} + \frac{1}{\overline{\gamma_e}} \right)^{-k-1} + \frac{e^{\frac{1}{\overline{\gamma_{je,l}}} - \frac{2}{\overline{\gamma_{je,l}}(\delta_i+1)}}}{\Gamma(N)(\eta_r \Omega_r)^N} \frac{\pi \gamma_{th}^N}{2N_0} \sum_{i=0}^{N_0} \left(\frac{\delta_i + 1}{2} \right)^{N-1} \sqrt{1 - \delta_i^2} \frac{N!}{\overline{\gamma_e}} \left(\frac{\gamma_{th}(\delta_i+1)}{2\eta_r \Omega_r} + \frac{1}{\overline{\gamma_e}} \right)^{-N-1} \\[2em]
\displaystyle - \sum_{k=0}^{N-1} \frac{\gamma_{th}^k}{k!(\eta_r \Omega_r)^k} \sum_{n=1}^{\infty} \mathrm{T} \left(n(k+n-1)! \left(\frac{\gamma_{th}}{\eta_r \Omega_r} + \frac{1}{\overline{\gamma_e}} \right)^{-(k+n)} - \frac{(k+n)!}{\overline{\gamma_e}} \left(\frac{\gamma_{th}}{\eta_r \Omega_r} + \frac{1}{\overline{\gamma_e}} \right)^{-(k+n)-1} \right) \\[2em]
\displaystyle - \frac{e^{\frac{1}{\overline{\gamma_{je,l}}} - \frac{2}{\overline{\gamma_{je,l}}(\delta_i+1)}}}{\Gamma(N)(\eta_r \Omega_r)^N} \frac{\pi \gamma_{th}^N}{2N_0} \sum_{i=0}^{N_0} \sum_{n=1}^{\infty} \left(\frac{\delta_i + 1}{2} \right)^{N-1} \sqrt{1 - \delta_i^2} \\[2em]
\displaystyle \times \mathrm{T} \left(n(N+n-1)! \left(\frac{\gamma_{th}(\delta_i+1)}{2\eta_r \Omega_r} + \frac{1}{\overline{\gamma_e}} \right)^{-(N+n)} - \frac{(N+n)!}{\overline{\gamma_e}} \left(\frac{\gamma_{th}(\delta_i+1)}{2\eta_r \Omega_r} + \frac{1}{\overline{\gamma_e}} \right)^{-(N+n)-1} \right)
\end{pmatrix}
$$

$$(39)$$

3.2 Asymptotic Behavior Analysis

In order to reveal further realization of the network performance, the asymptotic behavior is examined at high SNR regime ($\eta_s \to \infty$), and the diversity order of the network is obtained.

Theorem 5. *The asymptotic formula for the SOP of the network is denoted as*

$$
P_{\text{sec}}^{\infty} \approx \frac{\alpha_s^M}{M! \eta_s^M} (\gamma_{th} - 1)^M + \left(\frac{\alpha_s^M}{M! \eta_s^M} (\gamma_{th} - 1)^M + 1 \right)
$$

$$
\times \frac{\gamma_{th}^N}{(\eta_r \Omega_r)^N} \left(\frac{1}{N!} - \frac{e^{\frac{1}{\overline{\gamma_{je,l}}}}}{(N-1)!} \frac{\pi}{2N_0} \sum_{i=0}^{N_0} \left(\frac{\delta_i + 1}{2} \right)^{N-1} e^{-\frac{2}{\overline{\gamma_{je,l}}(\delta_i+1)}} \sqrt{1 - \delta_i^2} \right) \qquad (40)
$$

$$
\times \left(N! \left(\frac{1}{\overline{\gamma_e}} \right)^{-N} - \sum_{n=1}^{\infty} \mathrm{T} \left(n(N+n-1)! - (N+n)! \right) \left(\frac{1}{\overline{\gamma_e}} \right)^{-N-n} \right)
$$

Proof. At high SNR regime, expanding the exponential function using Maclaurin series expansion [31], the asymptotic formulas of $F_{\gamma_{sr}}$ and $f_{\gamma_{rd}}$ are given as

$$
F_{\gamma_{sr}}(x) \approx \frac{\alpha_s^M}{M! \eta_s^M} x^M \qquad (41)
$$

and

$$
f_{\gamma_{rd}}(x) \approx \frac{x^{N-1}}{(N-1)!(\eta_r \Omega_d)^N}. \qquad (42)
$$

Base on (16) and (42), the asymptotic expressions of (37) can be formulated as

$$F_A(z) \approx \frac{z^N}{\left(\eta_r \Omega_r\right)^N} \left(\frac{1}{N!} - \frac{e^{\frac{1}{\overline{\gamma}_{je,l}}}}{(N-1)!} \frac{\pi}{2N_0} \sum_{i=0}^{N_0} \left(\frac{\delta_i+1}{2}\right)^{N-1} e^{-\frac{2}{\overline{\gamma}_{je,l}(\delta_i+1)}} \sqrt{1-\delta_i^2} \right). \tag{43}$$

Substituting (34) and (43) into (36), after some algebra processing, the asymptotic formula of $F_{\gamma_d}(\gamma_{th})$ can be acquired as

$$F_{\gamma_d}(\gamma_{th}) \approx \left(N! \left(\frac{1}{\overline{\gamma}_e}\right)^{-N} - \sum_{n=1}^{\infty} T\left(n(N+n-1)! - (N+n)!\right) \left(\frac{1}{\overline{\gamma}_e}\right)^{-N-n} \right). \tag{44}$$

Then, combining (41), (44) and (25), (40) can be derived.

Corollary 1. The diversity order of the system at high SNR regime can be obtained by the following derivation.

$$d = -\lim_{\eta_s \to \infty} \frac{\log\left(P_{sec}^{\infty}\right)}{\log \eta_s} = \begin{cases} M, & M < N \\ M = N, & M = N \\ N, & M > N \end{cases} \tag{45}$$

Remark 1. From Corollary 1, it is observed that the diversity order of the system at high SNR regime is different in different system configurations, represented as $\min\{M,N\}$. This is to say that the average SNR increase is helpful for the improvement of the system secrecy performance, but it is also subject to the system configuration (the number of transmit/receive antennas).

3.3 Throughput Analysis

To further evaluate the secrecy of the considered HSTRN, the system throughput is investigated in this work. According to pertinent literature [32], the throughput is defined as

$$R_{thr} = \frac{C_{th}}{2} \times \left(1 - P_{sec}\left(C_{th}\right)\right), \tag{46}$$

where the $\frac{1}{2}$ denotes the two phases of the communication process, and $P_{sec}\left(C_{th}\right)$ can be acquired from the preceding equation. Then, invoking (39) into (46), the system throughput expression can be derived accordingly.

4. Numerical and Simulation Results

Numerical results from the preceding derivations are showed in this section. For purpose of validating the theoretical analysis results, computer simulations are performed by means of Monte-Carlo. Herein, the SOP performance and throughput analysis are explored based on different fading channel settings, and $\eta_s = \eta_r$ is set as transmit SNR. Unless otherwise described, the setting parameters of this work are shown as **Table 1** [9,32,33].

Table 1. Table of parameter settings

Heavy shadowing parameters of Shadowing-Rician fading	$m_s = 1$, $b_s = 0.063$, $\Omega_s = 0.0007$
Average shadowing parameters of Shadowing-Rician fading	$m_s = 5$, $b_s = 0.251$, $\Omega_s = 0.279$
Average power of the $R - D_N$ link	$\Omega_d = 1$
Average SNR of the wiretap link	$\overline{\gamma_{re}} = 1dB$
Average SNR of the jamming link	$\overline{\gamma_{je}} = 1dB$
Radius of relay coverage airspace	$D = 200m$
Height of relay	$h = 100m$
Path loss exponent	$v = 3$
Secrecy rate threshold	$C_{th} = 1$
Monte-Carlo simulations	10^6 iterations
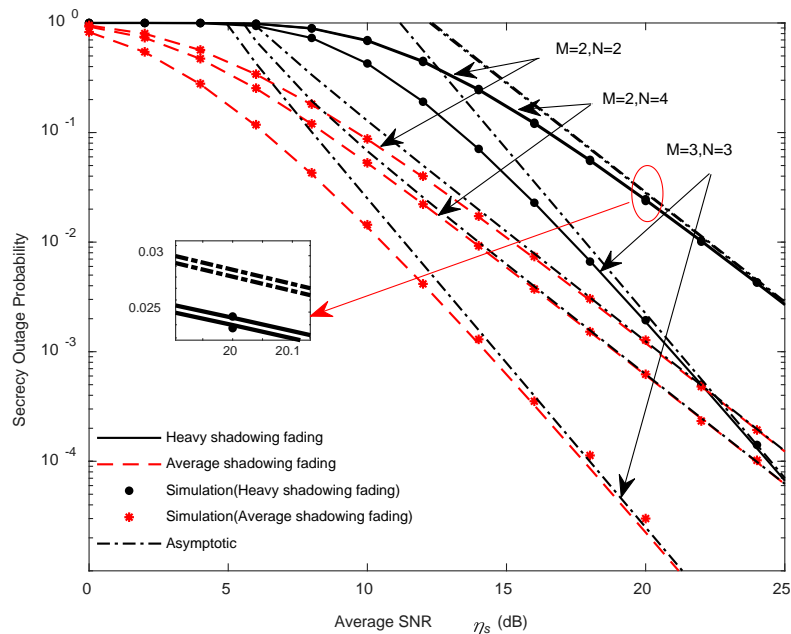
Fig. 3. SOP versus η_s for different system configurations.

Fig. 3 shows the SOP curves versus η_s for different system configurations and $S - R$ link in different Shadowing-Rician fading scenarios. The analytical and asymptotic SOP curves are drawn respectively according to (39) and (40). The theoretical numerical curves keep complete consistency with the computer simulation curves. Simulation results are obtained through 10^6 Monte-Carlo simulations, which provide a further verification of the theoretical analysis. The analytical and asymptotic SOP curves almost overlap at moderate-to-high SNR regime. As can be observed, for different system configurations (here referring the antennas number at transmit and receive node), the SOP performance gets better with the SNR increasing, and the SOP in average shadowing scenario is always better than heavy shadowing scenario. Also, notice that the 3×3 ($M = 3, N = 3$) scenario outperforms the 2×4 scenario, which outperforms the 2×2 scenario. This agrees with (45). Moreover, the diversity order of 3×3 system is higher than 2×4 system, although they have the same total antennas number. Therefore, the same antennas number at transmit and receive node is a preferable choice, and

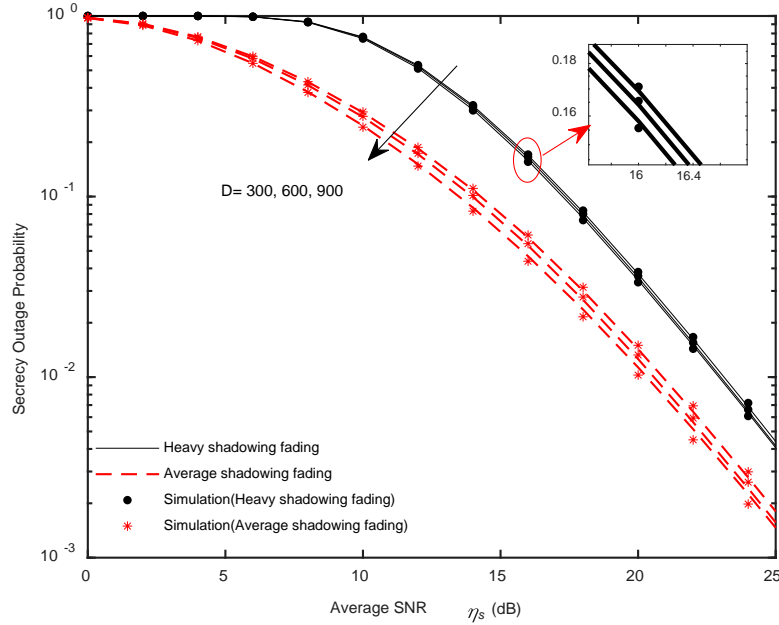this may be quite a practical result from an engineering viewpoint.

Fig. 4. SOP versus η_s for different D.

Fig. 4 plots the SOP curves for the 2×2 scenario versus η_s for different radius of the relay coverage airspace in different shadowing scenarios of Shadowing-Rician fading. Herein, $\overline{\gamma_{re}} = 10dB$ and $\overline{\gamma_{je}} = 5dB$. From the figure, we can notice that the SOP performance is improved due to the increasing of relay coverage airspace. This results from the worse eavesdropping channels, in which more path loss is caused by longer distance between the relay and the eavesdropper.
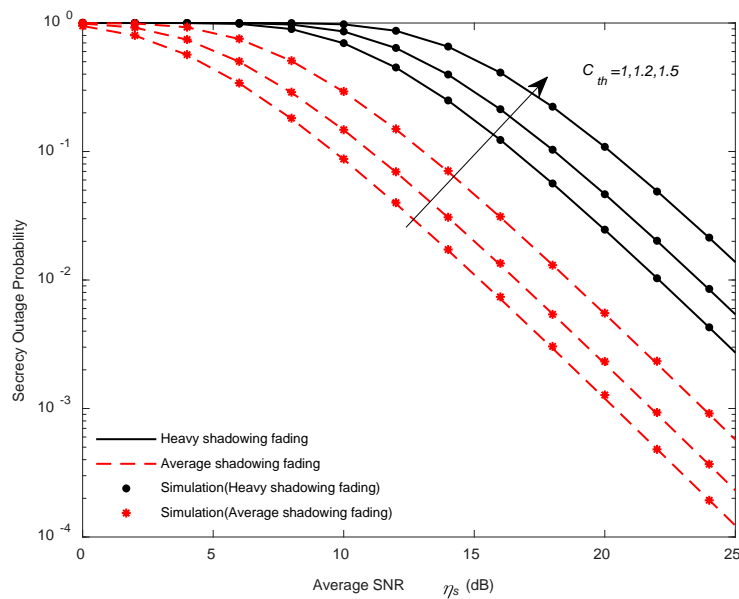
Fig. 5. SOP versus η_s for different C_{th}.

Fig. 5 plots the SOP curves for the 2×2 scenario versus η_s for different secrecy rate threshold C_{th} in different scenarios of Shadowing-Rician fading. As is expected, with the decreasing of secrecy rate threshold, the SOP performance improvement of the considered HSTRN is very obvious. However, the achieve order of the network keeps unchanged despite C_{th} increasing.
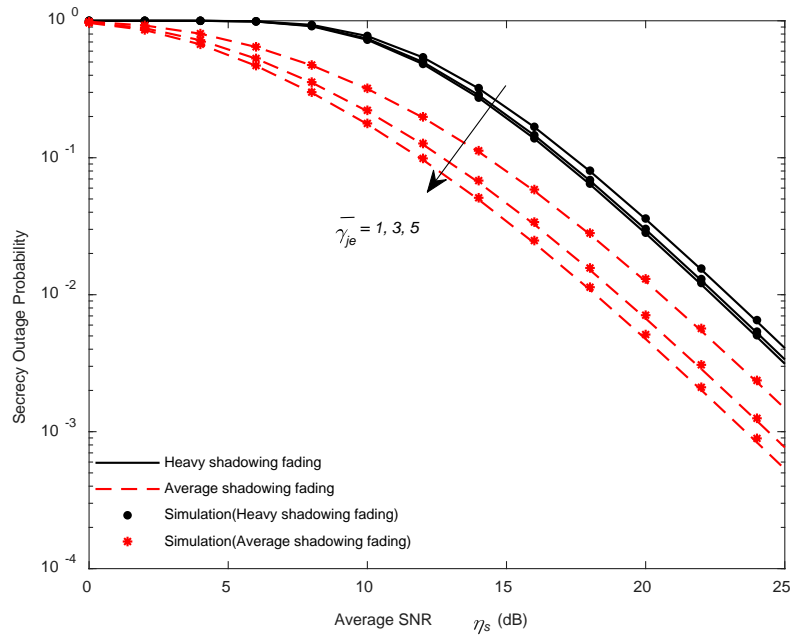

Fig. 6. SOP versus η_s for different $\overline{\gamma_{je}}$.

Fig. 6 plots a comparison of the SOP performance in the 2×2 scenario versus η_s for different $\overline{\gamma_{je}}$ in different fading scenarios. Here, we suppose $\overline{\gamma_{re}} = 5dB$. As shown in the figure, the network has a better SOP performance due to the SNR increasing of the jamming link. This can attribute to the jamming signal, which can weaken the eavesdropper link. In other word, the jamming signal has a great effect on the secrecy performance improvement of the network.
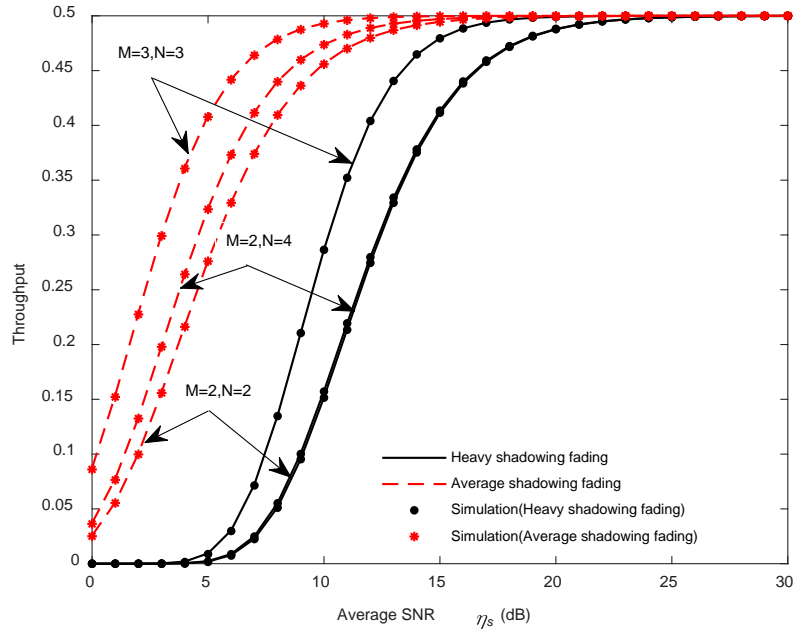
Fig. 7. System throughput versus η_s for different system configurations.

Fig. 7 describes the system throughput versus η_s for different system configurations in different fading scenarios. As can be noted, the throughputs for different system configurations increase with η_s increasing and then trend to a fixed constant. This result is due to the SOP performance which gets close to zero at high SNR regime. Obviously, the throughputs in average shadowing scenario are higher than heavy shadowing scenario. Moreover, the throughputs for 3×3 scenario in the three scenarios (2×2, 2×4, 3×3) are far superior to the other two, which agree well with the SOP performance presented in **Fig. 3**.

5. Conclusion

This work explores a physical layer secrecy investigation based on a multi-antenna HSTRN with jamming in the presence of spatial eavesdroppers. Assuming Shadowed-Rician fading for satellite link while Rayleigh fading for terrestrial link, eavesdropper link and jamming link, the theoretical expression for SOP has been deduced. Also, the diversity order of the network is obtained and the system throughput is explored. Then computer simulation is operated to validate the correctness of the theoretical analysis. The investigation illustrates that the channel fading scenario, the jammer, the relay coverage airspace and the number of transmit and receive antennas contribute much to the secrecy performance improvement of the considered HSTRN. Moreover, the location optimization of the relay in such system could be our further research.

Acknowledgement

References

[1] A. Vanelli-Coralli, G. Corazza, G. Karagiannidis, T. Mathiopoulos, and S. Scalise. "Satellite communications: Research trends and open issues," in *Proc. of International Workshop on Satellite and Space Communications*, Sept., 2007. Article (CrossRef Link)

[2] K. An, M. Lin, T. Liang, "On the performance of multiuser hybrid satellite-terrestrial relay networks with opportunistic scheduling," *IEEE Communications Letters*, vol. 19, no. 10, pp. 1722–1725, Oct. 2015. Article (CrossRef Link)

[3] K. F. Guo, B. N. Zhang, Y. Z. Huang, D. X. Guo, "Performance analysis of two-way satellite terrestrial relay networks with hardware impairments," *IEEE Wireless Communications Letters*, vol. 6, no. 4, pp. 430-433, Aug. 2017. Article (CrossRef Link)

[4] N. A. Sarker, M. F. Samad, "Capacity and outage performance analysis of secure cooperative RF-FSO relaying system in the presence of multiple eavesdroppers," *Physical Communication*, vol. 49, pp. 1–11, Dec. 2021. Article (CrossRef Link)

[5] B. Evans, M. Werner, E. Lutz, M. Bousquet, G. E. Corazza, G. Maral and R. Rumeau, "Integration of satellite and terrestrial systems in future multimedia communications," *IEEE Wireless Communication*, vol. 12, no. 5, pp. 72–80, Oct. 2005. Article (CrossRef Link)

[6] S. Kim, H. W. Kim, K. Kang and D. S. Ahn, "Performance Enhancement in Future Mobile Satellite Broadcasting Services," *IEEE Communications Magazine*, vol. 46, no. 7, pp. 118–124, July 2008. Article (CrossRef Link)

[7] Y. Bu, M. Lin, K. An, J. Ouyang, and C. Yuan, "Performance analysis of hybrid satellite-terrestrial cooperative systems with fixed gain relaying," *Wireless Personal Communications*, vol. 89, no. 2, pp. 427–445, March 2016. Article (CrossRef Link)

[8] S. Sreng, B. Escrig and M. L. Boucheret, "Exact Symbol Error Probability of Hybrid/Integrated Satellite-Terrestrial Cooperative Network," *IEEE Transactions on Wireless Communications*, vol. 12, no. 3, pp. 1310-1319, March 2013. Article (CrossRef Link)

[9] X. W. Li, Q. S. Wang, H. X. Peng, H. Zhang, and C. C, Cavalcante, "A unified framework for HS-UAV NOMA networks: Performance analysis and location optimization," *IEEE Access*, vol. 8, pp. 13329-13340, Jan. 2020. Article (CrossRef Link)

[10] X. W. Li, Q. S. Wang, Y. Liu, T. A. Tsiftsis, Z. G. Ding and A. Nallanathan, "UAV-aided multi-way NOMA networks with residual hardware impairments," *IEEE Wireless Communications Letters*, vol. 9, no. 9, pp. 1538–1542, May, 2020. Article (CrossRef Link)

[11] X. W. Li, M. L. Zhao, M. Zeng, S. Mumtaz, V. Menon, Z. G. Ding, and O. A. Dobre, "Hardware impaired ambient backscatter NOMA system: Reliability and security," *IEEE Transactions Communications*, vol. 69, no. 4, pp. 2723– 2736, April. 2021. Article (CrossRef Link)

[12] Digital video broadcasting (DVB); system specifications for Satellite services to Handheld sevices (SH) below 3 GHz, ETSI EN 102 585 V1.1.2, 2008.

[13] V. K. Sakarellos, C. Kourogiorgas, and A. D. Panagopoulos, "Cooperative hybrid land mobile satellite-terrestrial broadcasting systems: Outage probability evaluation and accurate simulation," *Wireless Personal Communications*, vol. 79, no. 2, pp. 1471–1481, July 2014. Article (CrossRef Link)

[14] M. Lin, Y. W. Jiang, J. Ouyang and K. An, "The performance of a hybrid satellite-terrestrial cooperative networks with interferences," *Acta Electronica Sinica*, vol. 46, no. 1, pp. 8–14, Jan. 2018. Article (CrossRef Link)

[15] N. I. Miridakis, D. D. Vergados, and A. Michalas, "Dual-Hop Communication over a Satellite Relay and Shadowed Rician Channels," *IEEE Transactions on Vehicular Technology*, vol. 64, no. 9, pp. 4031–4040, Sept. 2015. [Article (CrossRef Link)](#)

[16] K. An, M. Lin, T. Liang, J. B. Wang, J. Wang, Y. Huang and A. L. Swindlehurst, "Performance analysis of multi-antenna hybrid satellite-terrestrial relay networks in the presence of interference," *IEEE Transactions on Communications*, vol. 63, no. 11, pp. 4390–4404, Nov. 2015. [Article (CrossRef Link)](#)

[17] Wyner A D, "The wire-tap channel," *Bell System Technical Journal*, vol. 54, no. 8, pp. 1355–1387, Oct. 1975. [Article (CrossRef Link)](#)

[18] Q. Huang, M. Lin, K. An, J. Ouyang, and W. P. Zhu, "Secrecy performance of hybrid satellite-terrestrial relay networks in the presence of multiple eavesdroppers," *IET Communications*, vol. 12, no. 1, pp. 26–34, 2018. [Article (CrossRef Link)](#)

[19] V. Bankey and P. K. Upadhyay, "Physical layer security of multiuser multirelay hybrid satellite-terrestrial relay networks," *IEEE Transactions on Vehicular Technology*, vol. 68, no. 3, pp. 2488–2501, Jan. 2019. [Article (CrossRef Link)](#)

[20] X. Q. Wang, H. W. Zhang, and Z. Hou, "Physical Layer Secrecy Analysis of Multi-Hop Hybrid Satellite-Terrestrial Relay Networks with Jamming," *Wireless Communications and Mobile Computing*, vol. 2021, pp. 1–13, June 2021. [Article (CrossRef Link)](#)

[21] S. Yan, X. Wang, Z. Li, B. Li, and Z. Fei, "Cooperative jamming for physical layer security in hybrid satellite terrestrial relay networks," *China Communications*, vol. 16, no. 12, pp. 154–164, Dec. 2019. [Article (CrossRef Link)](#)

[22] Y. Yan, B. Zhang, D. Guo, S. Li, X. Wang, "Joint beamforming and jamming design for secure cooperative hybrid satellite-terrestrial relay network," in *Proc. of 25th Wireless and Optical Communication Conference*, July, 2016. [Article (CrossRef Link)](#)

[23] K. F. Guo, K. An, B. N. Zhang, Y. Z. Huang, and D. X. Guo, "Physical layer security for hybrid satellite terrestrial relay networks with joint relay selection and user scheduling," *IEEE Access*, vol. 6, pp. 55 815–55 827, Oct. 2018. [Article (CrossRef Link)](#)

[24] J. Ye, C. Zhang, G. Pan, Y. Chen, and Z. Ding, "Secrecy analysis for spatially random UAV systemsm" in *Proc. of 2018 IEEE Globecom Workshops*, Aug., 2018. [Article (CrossRef Link)](#)

[25] A. Abdi, W. C. Lau, M. S. Alouini, and M. Kaveh, "A new simple model for land mobile satellite channels: first-and second-order statistics," *IEEE Transactions on Wireless Communications*, vol. 2, no. 3, pp. 519–528, June 2003. [Article (CrossRef Link)](#)

[26] A. Pandey and S. Yadav, "Physical Layer Security in Cooperative AF Relaying Networks With Direct Links Over Mixed Rayleigh and Double-Rayleigh Fading Channels," *IEEE Transactions on Vehicular Technology*, vol. 67, no. 11, pp. 10615–10630, Nov. 2018. [Article (CrossRef Link)](#)

[27] L. Fan, N. Yang, T. Q. Duong, M. Elkashlan, and G. K. Karagiannidis, "Exploiting Direct Links for Physical Layer Security in Multiuser Multirelay Networks," *IEEE Transactions on Wireless Communications,* vol. 15, no. 6, pp. 3856–3867, June 2016. [Article (CrossRef Link)](#)

[28] E. R. Alotaibi and K. A. Hamdi, "Secure Relaying in Multihop Communication Systems," *IEEE Wireless Communications Letters*, vol. 20, no. 6, pp. 1120–1123, June 2016. [Article (CrossRef Link)](#)

[29] I. S. Gradshteyn, I. M. Ryzhik, *Tables of integrals, series and products*, 6th ed., Academic Press, New York, USA, 2000.

[30] D. D. Tran, D. B. Ha, "Secrecy performance analysis of QoS-based non-orthogonal multiple access networks over Nakagami-m fading," in *Proc. of 2nd International Conference on Recent Advances in Signal Processing, Telecommunications & Computing*, Jan., 2018. [Article (CrossRef Link)](#)

[31] P. L. Yeoh, M. Elkashlan and I. B. Collings, "Selection relaying with transmit beamforming: a comparison of fixed and variable gain relaying," *IEEE Transactions on Communications*, vol. 59, no. 6, pp. 1720-1730, June 2011. [Article (CrossRef Link)](#)

[32] K. F. Guo, K. An, B. N. Zhang, Y. Z. Huang, D. X. Guo, G. Zheng and S. Chatzinotas. "On the performance of the uplink satellite multi-terrestrial relay networks with hardware impairments and interference," *IEEE Systems Journal*, vol. 13, no. 3, pp. 2297-2308, Sept. 2019. [Article (CrossRef Link)](#)

[33] Loo C, "A statistical model for a land mobile satellite link," *IEEE Transactions on Vehicular Technology*, vol. 34, no. 3, pp. 122-127, Aug. 1985. Article (CrossRef Link)

Xiaoqi Wang received the B.Sc. degree from North University of China, in 2006 and the M.Sc. degree from China University of Mining and Technology-Beijing, in 2009. From 2009 until now, he has been working in School of Physics and Electronic Information Engineering, Henan Polytechnic University Jiaozuo, China, where he is currently pursuing the Ph.D. degree. His research interests include cooperative communication, satellite communication and physical layer security.

Zheng Hou received the M.Sc. degree from China University of Mining and Technology-Beijing, in 2014 and the Ph.D. degree from the Henan Polytechnic University, Jiaozuo, China, in 2020. From 2020 until now, he has been working in School of Surveying and Land Information Engineering, Henan Polytechnic University Jiaozuo, China. His research interests include geodetic data processing, the detection theory and method of crustal abnormal deformation information based on GNSS, and geodynamics.

Hanwei Zhang received the Ph.D. degree from the University of Chinese Acedemy of Sciences, Beijing, China, in 2004. From 2005 to 2007, he was a Postdoctoral Researcher with Yunnan Observatories, Chinese Academy of Sciences, Kunming, China. He is currently a professor at Henan Polytechnic University, Jiaozuo, China. His research interests include electromagnetic wave propagation theory, celestial reference systems and terrestrial reference systems, and earth rotation theory in space geodesy.